Journal of Hazardous Materials 308 (2016) 192–198

Contents lists available at ScienceDirect

Journal of Hazardous Materials

journal homepage: www.elsevier.com/locate/jhazmat

Rapid dehalogenation of pesticides and organics at the interface of reduced graphene oxide–silver nanocomposite

Dibyashree Koushik[a], Soujit Sen Gupta[a], Shihabudheen M. Maliyekkal[b], T. Pradeep[a,*]

[a] DST Unit of Nanoscience and Thematic Unit of Excellence, Department of Chemistry, Indian Institute of Technology Madras, Chennai 600036, India
[b] Environmental Engineering Division, School of Mechanical and Building Sciences, VIT University, Chennai Campus, Chennai, 600127, India

HIGHLIGHTS

- Preparation of reduced graphene oxide-silver nanocomposite (RGO@Ag).
- Dehalogenation of various POPs at reduced graphene oxide–silver nanocomposite (RGO@Ag).
- A two step mechanism involving degradation followed by the adsorption.
- Adsorption kinetics followed a pseudo-second-order rate equation.
- The material has high adsorption capacity and can be reused for multiple cycles.

GRAPHICAL ABSTRACT

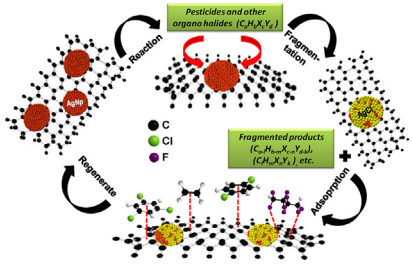

ARTICLE INFO

Article history:
Received 8 October 2015
Received in revised form
21 December 2015
Accepted 3 January 2016
Available online 11 January 2016

Keywords:
Reduced graphene oxide–silver nanocomposite (RGO@Ag)
Pesticide
Adsorption
Degradation
Water purification

ABSTRACT

This paper reports dehalogenation of various organohalides, especially aliphatic halocarbons and pesticides at reduced graphene oxide–silver nanocomposite (RGO@Ag). Several pesticides as well as chlorinated and fluorinated alkyl halides were chosen for this purpose. The composite and the products of degradation were characterized thoroughly by means of various microscopic and spectroscopic techniques. A sequential two-step mechanism involving dehalogenation of the target pollutants by silver nanoparticles followed by adsorption of the degraded compounds onto RGO was revealed. The composite showed unusual adsorption capacity, as high as 1534 mg/g, which facilitated the complete removal of the pollutants. Irrespective of the pollutants tested, a pseudo-second-order rate equation best described the adsorption kinetics. The affinity of the composite manifested chemical differences. The high adsorption capacity and re-usability makes the composite an excellent substrate for purification of water.

1. Introduction

Graphene, since its discovery [1] has witnessed a wide range of applications in the fields of biotechnology [2], catalysis [3,4], sensors [5] and electronics [6–8]. In contrast, its use in environmental clean-up has started gaining momentum only in recent years [9]. Reduced cytotoxicity [10,11], large surface area [12], availability of delocalized π-electrons [10], antibacterial properties [13] and tunable chemical properties [13–15] make graphene an ideal choice for purification of water [16–21]. Among the various pollutants present in water, pesticides and halogenated compounds require special attention due to their widespread occurrence in the environment [22–25], acute toxicity [26–28], and chemical diversity [29]. Most of the halogenated compounds are now listed under

* Corresponding author. Fax: +91 44 2257 0545x0509.
E-mail address: pradeep@iitm.ac.in (T. Pradeep).

http://dx.doi.org/10.1016/j.jhazmat.2016.01.004
0304-3894/

the category of persistent organic pollutants (POPs) and are highly susceptible to bioaccumulation in the food chain [30]. Efforts are made to detoxify and/or remove these POPs from water [31,32]. Recently, Maliyekkal et al. have proposed reduced graphene oxide (RGO) as a reusable substrate for the effective removal of pesticides such as chlorpyrifos, endosulphan and malathion from water [33]. The study showed unprecedented ability of RGO to remove these pesticides where adsorption is mediated through water. Liu et al. have shown that graphene-coated silica can be effectively used for the removal of organo phosphorus pesticides from water. The likely mechanism of adsorption was due to electron-donating abilities of the S, P, and N atoms and the strong π-bonding network of the benzene rings [34]. Wu et al. prepared graphene-based magnetic nanocomposites for the extraction of carbamate pesticides from environmental water samples by adsorption [35]. Very recent investigations by Gupta et al. have proved that graphene-silver composite does unusual dehydrohalogentation in which lindane is converted to trichlorobenzene [36]. Unlike graphene (supported and unsupported), this composite substrate enabled the degradation and subsequent adsorption of the products formed.

In this paper, we explore the versatility of reduced graphene oxide-silver nanocomposite (RGO@Ag) for dehalogenation. A diverse groups of pesticides (chlorpyrifos (CP), endosulfan (ES), dichlorodiphenyldichloroethylene (DDE)), chlorocarbons (carbon tetrachloride (CCl_4), chloroform ($CHCl_3$), dichloromethane (CH_2Cl_2)) and fluorocarbons (1,1,1,3,3,3-hexafluoro-2-propanol (HFP) and 1,1,1,2,2,3,3,4,4,5,5,6,6,7,7,8,8-heptadeca fluoro-10-iodo decane (HFID)) have been dehalogenated by the composite, in water at concentrations of relevance. We have also explored the likely mechanism of this chemistry. This work demonstrates that RGO@Ag is a versatile substrate and is capable of removing diverse pesticides and halogenated compounds in water at conditions of relevance to drinking water.

2. Experimental methods

2.1. Materials

Natural graphite flakes (95% of carbon) were obtained from Active Carbon India Pvt. Ltd. Ammonia (NH_3, 30%), sulfuric acid (H_2SO_4, 95–98%), and hydrochloric acid (HCl, 36%), were procured from Rankem Chemicals Pvt. Ltd., India. Phosphorus pentoxide (P_2O_5, 95%), hydrogen peroxide (H_2O_2, 98%) and hydrazine monohydrate ($N_2H_4.H_2O$, >99%) were purchased from SD Fine Chemicals Pvt. Ltd., India. Merck, India supplied potassium permanganate ($KMnO_4$, 98.5%). Potassium peroxydisulfate ($K_2S_2O_8$, 98%) was procured from Sisco Research Laboratories Pvt. Ltd., India. The pesticides and the halogenated organic samples were purchased from Sigma Aldrich. Ethanol (99.9%) and *n*-hexane (99.9%) were procured from Rankem Chemicals Pvt. Ltd. Stock solutions of the target pollutants (1000 mg/L) were prepared in ethanol and stored under refrigeration. Working concentrations of the pollutants were prepared by spiking appropriate volumes of the stock to the dispersion of the composite in water. All chemicals were of analytical grade and used as received. All solutions and suspensions were prepared in deionized water (DW), unless otherwise mentioned.

2.2. Synthesis of RGO@Ag

Graphene oxide (GO) was synthesized from graphite powder through a chemical process similar to the modified Hummers method [37]. RGO was synthesized through chemical reduction of GO [38–40]. Synthesis procedures are elaborated in S1 of the supplementary data along with basic characterization which includes TEM, AFM and Raman spectroscopy. Working concentrations of RGO were prepared by serial dilution to 0.01 wt% of RGO dispersion. A calculated amount of $AgNO_3$ (0.01, 0.05 and 0.1 mM) was added to the RGO dispersion to obtain RGO@Ag composite. These solutions were kept undisturbed for about 24 h at room temperature ($30 \pm 2\,^{\circ}C$) and atmospheric pressure to facilitate the formation of Ag NPs on the RGO surface. The composite was dialyzed by a cellulose membrane (dialysis tube, Sigma–Aldrich) to remove unwanted ions. The as-prepared composites were stored in a glass bottle for further use.

2.3. Adsorption experiments

Adsorption studies were performed in batch reactors of 20 mL capacity at room temperature ($30 \pm 2\,^{\circ}C$). The working volume and the pH of the solution were maintained at 5 mL and at 7 ± 0.1, respectively. The required volume of the stock solution (1000 mg/L) was spiked into the reactor to achieve the pre-decided concentration of the target pollutant. The working solution has a small amount of ethanol (<0.5% by volume), which was used to prepare the stock solutions of the target pollutants. Solid–liquid separation was performed with a 200 nm cellulose acetate filter paper. The residual concentration of the solute and the by-products were analysed using a gas chromatograph (GC) (PerkinElmer, Clarrus 680) equipped with an electron-capture detector (ECD). The analysis conditions involved an injector temperature of 200 °C, an injection rate of 12.5 pts/s, a run time of 38.5 min, and a carrier gas flow rate of 1 mL/min. The contact time and the RGO@Ag dose were varied to study their effect on the removal of the target pollutants. All experiments were conducted in triplicate and average values are reported. The samples were analyzed immediately after the reaction. Control experiments were run in parallel to assess any possible natural degradation of the pollutants.

2.4. Instrumentation

A PerkinElmer Lambda 25 UV/vis spectrophotometer was used to measure the UV/vis spectrum. XPS measurements were done with an Omicron ESCAProbe spectrometer with polychromatic Mg Kα X-rays ($h\nu = 1253.6$ eV). Raman spectra of RGO and GO were collected by a confocal Raman spectroscope (WiTec GmbH CRM 200). The samples were imaged by a high-resolution transmission electron microscope (HRTEM) with a UHR polepiece (JEOL 3011, 300 kV) with an energy-dispersive spectroscopy (EDS) attachment (Oxford). A scanning electron microscope (SEM) equipped with EDS (FEI Quanta 200, Czechoslovakia) was used to record the surface morphology, elemental composition and the elemental map of the samples. Residual concentration of the samples in water was analyzed by GC-ECD (PerkinElmer, Clarus 680, coupled with electron-capture detector). The mass spectrometric studies were done by an electrospray system, 3200 Q-TRAP LC/MS/MS (Applied Biosystems).

3. Results and discussion

RGO@Ag was characterized using both spectroscopic and microscopic techniques. We present essential details of these studies below. The TEM image in Fig. 1 shows the presence of Ag NPs on the RGO sheet. The folds on the RGO sheets are marked in the figure with white arrows and the black dots on it represent the Ag NPs formed on the sheet. The Ag NPs formed are of uniform size (5 nm) and the lattice separation of 0.232 nm (shown in Fig. 1(a1) and an expanded image in Fig. 1(a2)) confirm that the nanoparticles formed exhibit the (1 1 1) lattice plane of silver. The XPS survey spectrum of the composite in supplementary data Fig. S2 shows the presence of carbon, oxygen and silver. The deconvoluted C1s spectrum shows the presence of oxygen functionality (C1s at 285.6

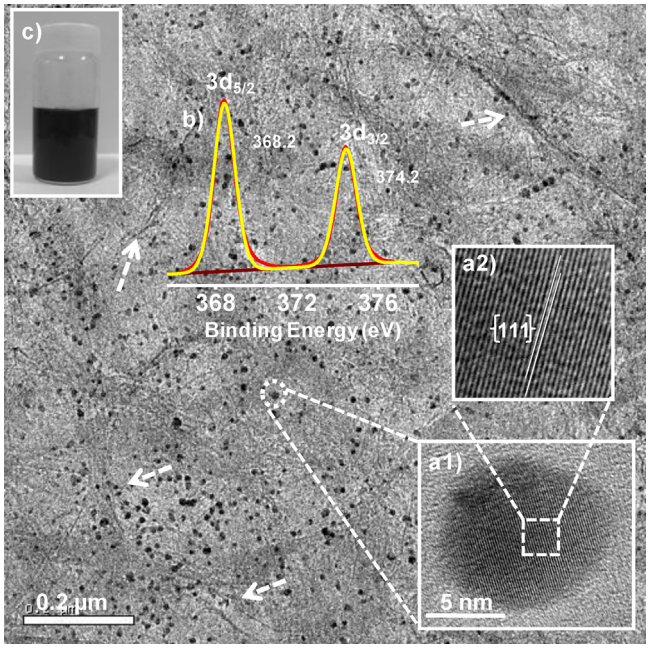

Fig. 1. TEM image of RGO@Ag composite; the folding of the RGO sheets is marked with white arrows. Insets: (a1) HRTEM image of a single nanoparticle, (a2) expanded portion from (a1) showing a lattice spacing of 0.232 nm corresponding to the (1 1 1) lattice plane, (b) deconvoluted XPS spectrum of Ag in the composite and (c) photograph showing the dispersed nature of the composite.

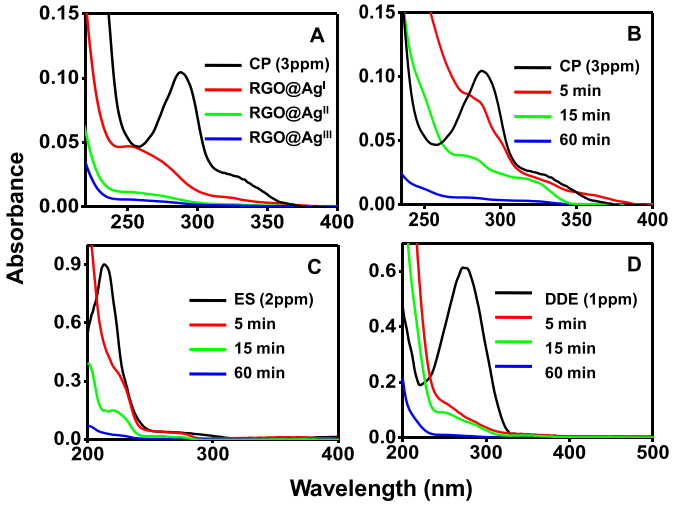

Fig. 2. UV/vis spectra showing the removal of (A) CP (at different concentrations of Ag NPs on RGO@Ag), (B) CP, (C) ES and (D) DDE at different time intervals by RGO@Ag^{II} (termed as RGO@Ag) in the text.

and 288.6 eV, due to C—O and C═O) along with C═C at 284.5 eV as the major components, as expected for sulphonated RGO (shown in Supplementary data Fig. S2). The deconvoluted Ag3d XPS spectrum is shown in Fig. 1b and the Ag3d$_{5/2}$ peak around 368.2 eV suggests that the oxidation state of silver is zero. This further confirms the presence of uncapped Ag NPs on the RGO sheet. Preparation of RGO@Ag and its characterization has been reported elsewhere [9,41]. The photograph in Fig. 1c shows the dispersed nature of the composite, which remains stable even after 6 months of preparation. The UV/vis spectrum of the dispersion in supplementary data Fig. S3 shows the presence of two peaks, one at 267 nm which characterizes RGO and the other at 420 nm, due to the plasmonic resonance of Ag NPs present on the RGO@Ag composite. These results confirm the formation of RGO@Ag composite.

This RGO@Ag composite was tested for the removal of various pollutants from water, which included different pesticides and halogenated compounds. Fig. 2 shows the UV/vis spectrum for the removal of different pesticides, which were of concern in our studies. The decrease in the intensity of the peaks with respect to time ensures that the pesticides are removed from water when treated with RGO@Ag composite. Fig. 2A shows the efficiency of RGO@Ag composite for the removal of CP from water (3 ppm) after 60 min of reaction when different loading percentage of silver was taken in the composite. When 0.01, 0.05, 0.1 mM of precursor $AgNO_3$ was used in 0.01 wt% of RGO solution, the resulting composites are termed as RGO@Ag^{I}, RGO@Ag^{II} and RGO@Ag^{III}, respectively. It was seen that RGO@Ag^{II} was better in performance than RGO@Ag^{I}, but there was no improvement for RGO@Ag^{III}. So, RGO@Ag^{II} (termed as RGO@Ag throughout the text) was taken as the standard for all other reactions unless mentioned. Time-dependent UV/vis spectra were taken for CP, which shows that CP has a characteristic peak around 297 nm. When CP was reacted with RGO@Ag composite, decrease of the peak height with respect to time indicates that CP is removed from water (Fig. 2B). Similarly, in Fig. 2C, 2 ppm of ES was taken, having a peak at 236 nm. When treated with the RGO@Ag composite, time dependent UV/vis shows that ES was removed from the solution as a function of time. A complete removal was observed after 60 min of reaction. Similar observation was also made for DDE (1 ppm) which shows a peak maximum around 285 nm as shown in Fig. 2D (black trace) and it was removed after reaction with RGO@Ag composite within 60 min.

Similarly, removal of pesticides (1 ppm) from water was confirmed by means of GC-ECD technique, which is one of the best tools for quantitative estimation of halogenated compounds. For CP, we got a peak at a retention time of 12.2 min (Fig. 3Aa), which disappeared completely after 1 h of reaction with RGO@Ag (5 mL in each case) composite (Fig. 3Ab). The time-dependent GC-ECD for CP is presented in supplementary data Fig. S4, which shows that there was degradation of CP followed by complete removal of the degraded products. Similarly, DDE has a peak at a retention time of 13.7 min, which was also removed during 1 h of reaction as shown in Fig. 3B. ES and HFID removal are shown in Fig. 3C and D, which have peaks at 13.2 and 4.5 min, respectively. The corresponding structures of the compounds are given in the insets. The GC-ECD data for CCl_4, $CHCl_3$, CH_2Cl_2 and HFP before and after the reaction with the composite are shown in supplementary data Fig. S5.

Mass spectrometry is one of the best available tools to detect organic molecules. As mentioned previously, the RGO@Ag composite degrades the organohalides first into smaller fragments and then these fragments get adsorbed onto the RGO sheet. Therefore, we used ESI MS to characterize these molecules. Fig. 4Aa represents the ESI MS of DDE which shows a peak at m/z 283 due to $C_{14}H_8Cl_3^+$. The isotope distribution of the peak is shown in the inset of the figure which arises because of the presence of three Cl atoms. Fig. 4Ab shows the mass spectrum of the fragments formed after the reaction of DDE with RGO@Ag. A peak around m/z 145 represents the formation of dichlorobenzene in the reaction mixture. The isotope distribution of the peak is presented in the inset which matches perfectly with the theoretical distribution of $C_6H_4Cl_2^+$. Similarly, Fig. 4Ba presents the MS of CP, with a molecular ion at m/z 351 in the positive mode. The corresponding isotope distribution is shown in the inset of the figure. The product formed shows peaks at m/z 258 and 179, corresponding to $C_5HCl_3NOPS^+$ and $C_5HCl_3N^+$, respectively (Fig. 4Bb). It was seen that RGO@Ag is indeed degrading halogenated compounds; the ESI MS of ES is shown in Fig. S6 (Supplementary data) along with that of the fragmented product.

To characterize RGO@Ag composite after reaction, TEM image of the material was taken as shown in Fig. 5A. The wrinkles on RGO sheets are marked with white arrows and the black dots represent

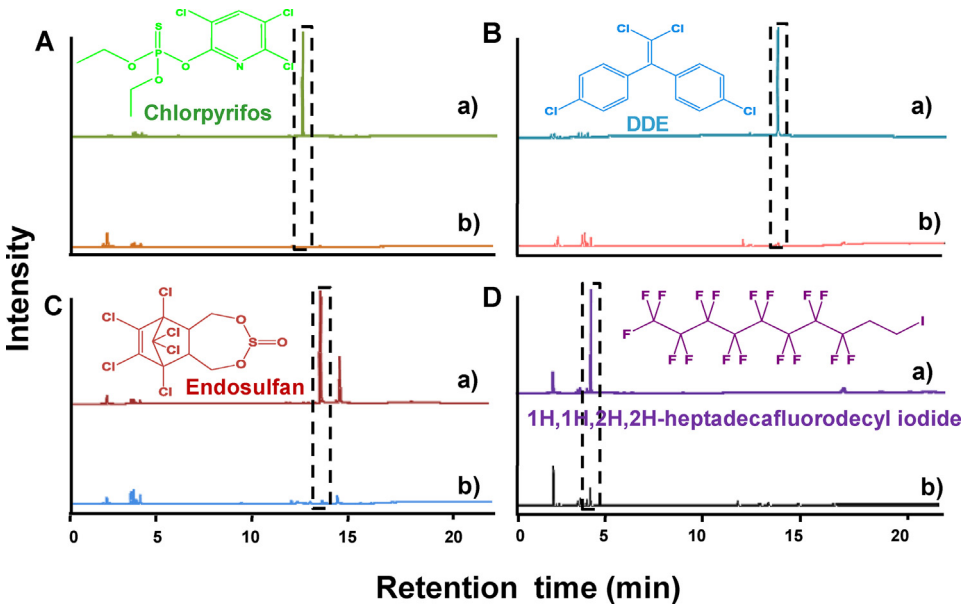

Fig. 3. GC-ECD data for the removal of (A) CP, (B) DDE, (C) ES, (D) HDIF after reaction with RGO@Ag. In all cases, the reaction time was 1 h. The traces a and b correspond to the traces before and after the reaction. The disappearance of the respective pollutant is shown by the dotted boxes.

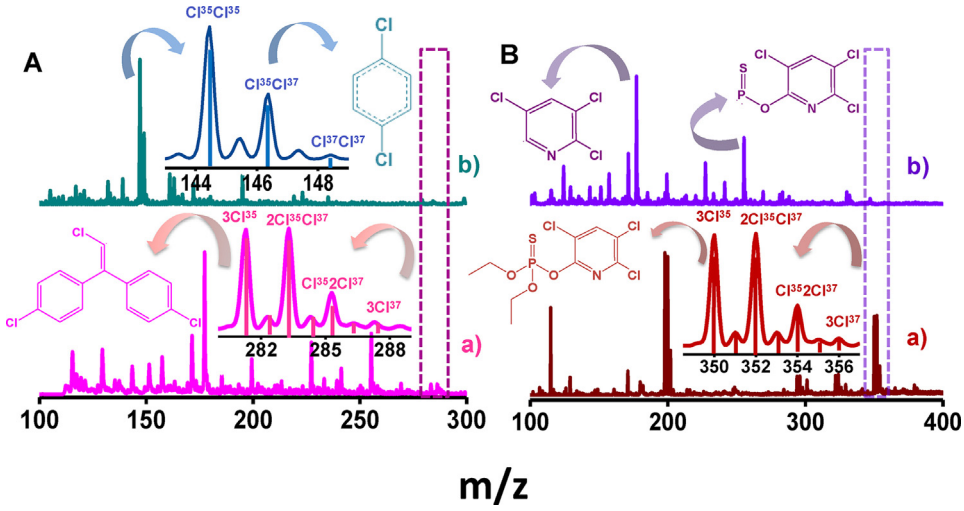

Fig. 4. ESI MS of (A) DDE (pink trace (a)) and the product (olive trace (b)) and (B) CP (brown trace (a)) and the product (violet trace (b)). Inset shows the isotope distribution of chlorine along with the corresponding molecular structure of the analytes. Isotope distribution is indicated on the spectrum. The pollutant region is highlighted by the dotted boxes. (For interpretation of the references to colour in this figure legend, the reader is referred to the web version of this article.)

Ag NPs as previously shown. Upon closer examination of the lattice spacing of the particles, it was seen that two different types of lattice spacing are present. One at 0.242 nm is due to the (1 1 1) lattice of silver and the other at 0.324 nm is due to the (1 1 1) lattice of AgCl [42] (Fig. 5A1). This shows that Ag NPs on RGO@Ag composite are responsible for the degradation of halogenated compounds. Expanded views of the HRTEM images are shown in the inset of Fig. 5A(a and b). Ag NPs on the composites facilitate the dehalogenation of the target compounds and get converted to AgCl as confirmed by elemental mapping. For elemental mapping, a bigger particle was chosen deliberately as shown in Fig. 5B. The elemental maps show the presence of Ag in RGO@Ag composite. Chlorine and phosphorus come from CP which got adsorbed onto the composite. Fig. 5C represents the TEM-EDS of the composite after reaction with CP. XPS of the composite was taken after reaction with CP; the survey spectrum is represented in supplementary data Fig. S7. The C1s spectrum is shown in Fig. 5D which on deconvolution shows the presence of peaks centred around 284.5, 285.7 and 288.7 eV corresponding to C=C, C—O and C=O/O—C—O, respectively. The deconvoluted Ag3d spectrum is shown in Fig. 5E. A change in the oxidation state of silver from Ag(0) to Ag(I) corresponding to the formation of AgCl from Ag NPs is seen. The shift of $Ag3d_{5/2}$ peak from 368.2 eV to 367.4 eV after reaction represents the conversion of Ag(0) to Ag(I). This is shown in supplementary data Fig. S8. Note that in Ag, oxidation leads to reduction in binding energy of 0.8 eV [43]. The presence of $Cl2p_{3/2}$ and $Cl2p_{1/2}$ peaks at 199.2 and 200.8 eV confirms the dehalogenation of the halogenated pollutants when it reacts with RGO@Ag; i.e, it confirms the presence of metal chloride (AgCl), whereas the presence of peak at higher binding energy (201.1 and 202.7 eV) represents the presence $Cl2p_{3/2}$ and $Cl2p_{1/2}$ of organic chloride. The deconvoluted O1s and S2p peaks are shown in supplementary data Fig. S7. The SEM-EDS spectrum of the composite after reaction with DDE and ES are shown in supplementary data Fig. S9A and B.

The schematic presented in Scheme 1 shows two-step mechanistic cycle for the removal of pesticides and other halogenated

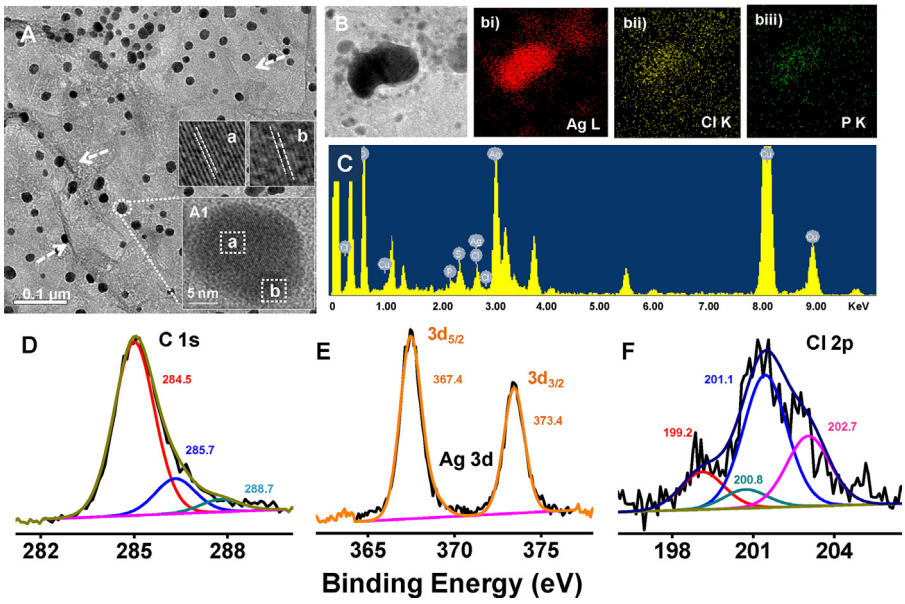

Fig. 5. Data corresponding to RGO@Ag after the reaction. (A) TEM image, (A1) HRTEM image of a single Ag NP, (a and b) expanded views of the HRTEM image presented in A1 showing the lattice spacing due to Ag (1 1 1). (B) TEM image of Ag NPs of 50 nm size, (bi–biii) elemental maps of Ag, Cland P, respectively. (C) TEM-EDS, (D–F) Deconvoluted XPS spectrum of C1s, Ag3d and Cl2p.

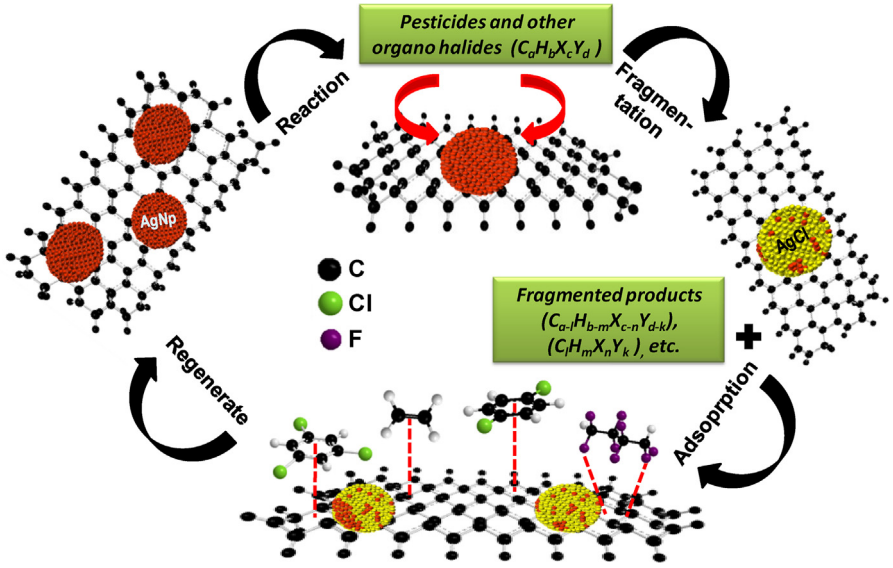

Scheme 1. Schematic showing the events involved in the removal of the pesticides and organo-halides from water.

pollutants from water. The first step involves the reaction of Ag NPs with the halogenated compounds at the interface of RGO@Ag and simultaneous degradation of the pollutant into smaller fragments by Ag NPs. In this course, Ag NPs are converted to AgCl. The next step comprises of the removal of the fragmented products from water by adsorption on the RGO sheet by π–π interactions arising between π electrons of RGO and aromatic compounds. Interactions such as van der Waals forces or hydrogen bonding are also likely. The composite once used can be regenerated and used multiple times. This is discussed later in the text.

4. Reaction kinetics

Experiments were performed to understand the time dependent removal of the pollutants individually and in combination. Initial concentrations of the target pollutants were maintained at 2 mg/L. The data are shown in Fig. 6A. We see that around 90% of the target species were removed from the aqueous medium in the first 30 min of the commencement of the adsorption process. Complete removal of the pollutants was achieved in <3 h of contact time. Two well-known mathematical models including Lagergren pseudo-first-order [44] and Ho's pseudo second-order reaction rate [45,46] models were used to describe the kinetic data. The mathematical representations of these models are given below.

$$\text{Pseudo-first-order equation } q_t = q_e(1 - e^{-k_1 t}) \quad (1)$$

$$\text{Pseudo-second-order equation } q_t = \frac{q_e^2 k_2 t}{1 + q_e k_2 t} \quad (2)$$

Where, q_e and q_t represents the amount of target pollutants removed per unit gram of RGO@Ag at equilibrium and at any time t (h), respectively, respectively. k_1 (1/h) and k_2 (g/mg h) are the first-order and second-order rate constants, respectively.

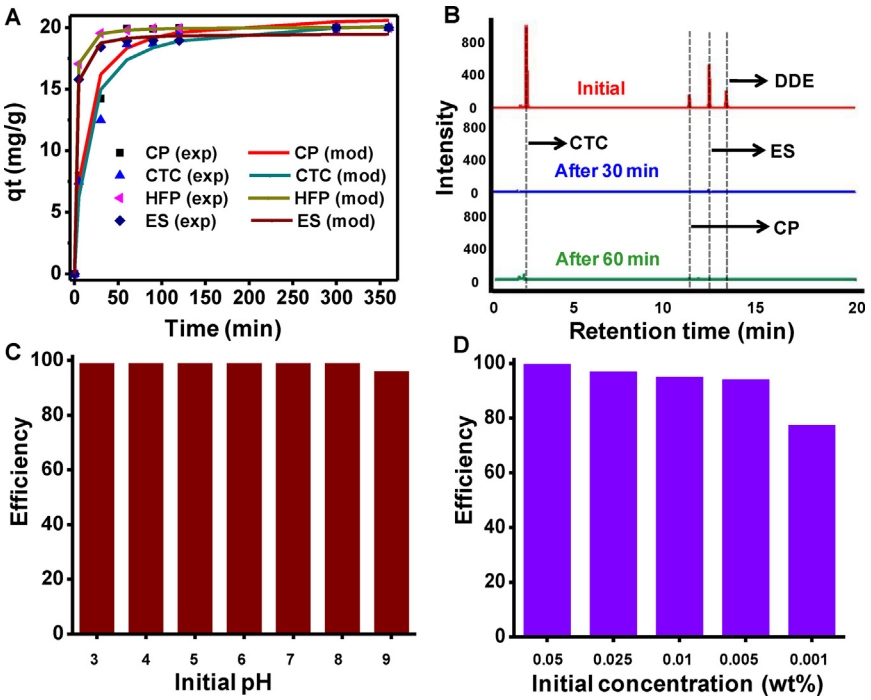

Fig. 6. (A) Kinetic data showing the pseudo second-order fit for the individual pollutants, (B) The removal rate when a group of pollutants (CP, ES, CCl_4 and DDE) was taken, (C) the effect of initial pH and (D) removal efficiency as a function of initial concentration of the composite in water. (For interpretation of the references to colour in the text, the reader is referred to the web version of this article.)

Table 1
Estimated model parameters of pseudo second-order reaction.

Pollutants	K_2 (g/mg h)	q_e (mg/g)	RMSE	X^2
CP	0.0052	21.1000	0.9960	0.4740
ES	0.0415	19.5300	0.3500	0.0510
CCl_4	0.0042	20.7400	1.1080	0.7770
HFP	0.0563	20.0900	0.0030	0.0004

Pseudo-second-order fits along with the experimental data are shown in Fig. 6A. The model parameters are summarized in Table 1. The corresponding first-order fits and the model parameters are shown in Supplementary data Fig. S10. As evident from low RMSE (root mean squared error) and Chi-square (χ^2) values, the pseudo-second-order equation describes the data better. The rate of adsorption significantly varies with the type of pollutants studied. Maximum rate was observed in the case of HFP followed by ES, CP and CCl_4. Similar removal patterns were observed even when a mixture of these compounds were spiked to RGO@Ag dispersion (Fig. 6B). The high rate of reaction of HFP to RGO@Ag can be attributed to the high electronegativity of fluorine. The interaction between silver and easily accessible chloride ions in ES may the reason for the relatively high rate of removal of ES over CP. Unlike the other compounds, the aliphatic nature and strong C—Cl bond in CCl_4 makes the pollutant less accessible contributing to the slow rate of reaction.

Fig. 6B shows the removal kinetics when a group of pollutants was used (i.e, CP, ES, CCl_4 and DDE) at initial concentration of 1 ppm each (Fig. 6B, red trace). 5 mL of 0.01 wt% RGO@Ag was taken and the pollutant mixture was spiked. The reaction was carried for an hour and two sets of readings were taken at 30 and 60 min. As expected, ES had fastest reaction rate followed by CP, DDE and CCl_4. The removal efficiency of the pollutants did not vary with pH of the initial solution, in the range of 3–9 (Fig. 6C). The pH of the solution was maintained acidic by using HNO_3 and basic by $NaHCO_3$. The pH was not varied above 9 as it results in silver hydroxide. It was also seen that the removal capacity increases with dilution of RGO@Ag solution as shown in Fig. 6D. The capacity that is considered here is the amount of target pollutant removed per gram of RGO@Ag (i.e. unit uptake capacity). The unit uptake capacities of the target pollutants increased with decreasing dose of the composite. This can be due to increased mass transfer at higher adsorbate to adsorbent ratio. Free surface area of the composite increases with dilution because of better separation of RGO sheets at higher dilution, which enhances the free adsorption/reaction sites and hence, increases the removal capacity. To check the maximum adsorption capacity of the composite for each pollutant, 5 mL of 0.001 wt% of RGO@Ag solution was taken and 2 ppm of the pollutant was spiked on it and after 2 h, the reaction was stopped and the solution was analyzed in GC-ECD. The removal capacity was calculated in mg/g of the pollutant removed/g of composite. The maximum removal capacity of the pollutant is reported in Table S11 of Supplementary data. The proposed dehalogenation chemistry and subsequent removal of the degraded products from water does not occur on RGO or Ag NPs in isolation, as revealed from separate experiments [36].

The RGO can be regenerated and reused multiple times. Firstly, the composite was stirred with hexane for 10 min, filtered and dried in ambient conditions at room temperature. Then, the composite was taken and concentrated ammonia solution was added to it and was sonicated. The pre-formed AgCl after the reaction dissolved in the solution leaving behind RGO. This RGO was further filtered, washed with DI water several times and was redispersed in water. A calculated amount of $AgNO_3$ (0.01, 0.05 and 0.1 mM) was added to RGO dispersion to obtain the RGO@Ag composite as discussed earlier. The performance of the composite was tested and the efficiency was found to be more than 95% even after 5 repeated uses.

5. Conclusion

The paper demonstrated the versatility of RGO@Ag composite in removing various group of pesticides and halogenated compounds in water. Unlike other graphene-based substrates studied

for the purpose, the proposed composites enable the degradation and complete removal of the pollutants from water. A two step mechanism involving the degradation of the pollutants by Ag nanoparticles followed by the adsorption of the reaction products onto the RGO sheet by $\pi-\pi$ interaction is proposed. The substrate is reusable and can be employed as an effective medium for removing pesticides and halogenated compounds present in water. This study would open an additional direction for the removal of POPs in water.

Acknowledgments

We thank the Nano Mission, Government of India operated by of the Department of Science and Technology (DST), for supporting the research program. SSG thanks the SERB, CII and Thermax India Pvt. Ltd. for a research fellowship. D.K. was a summer fellow from the Centre for Nanotechnology, Central University of Jharkhand, Ranchi, while this work was performed.

Appendix A. Supplementary data

Supplementary data available: Preparation of RGO and its basic characterization, XPS survey spectrum of RGO@Ag, UV/vis spectrum of RGO@Ag, time dependent GC-ECD showing complete removal of pesticide CP from water, GC-ECD showing the removal different compounds, ESI MS of endosulphan, XPS survey spectrum of the RGO@Ag composite after the reaction with CP, deconvoluted XPS spectrum of Ag in RGO@Ag before and after reaction with CP, SEM-EDS of RGO@Ag composite after the reaction with DDE and ES, pseudo-first-order kinetic plots for the adsorption of pesticides by RGO@Ag composites and the maximum removal capacity of the RGO@Ag composite for different pollutant in mg/g.

Supplementary data associated with this article can be found, in the online version, at http://dx.doi.org/10.1016/j.jhazmat.2016.01.004.

References

[1] A.K. Geim, K.S. Novoselov, The rise of graphene, Nat. Mater. 6 (2007) 183–191.
[2] Z. Liu, J.T. Robinson, X. Sun, H. Dai, PEGylated nanographene oxide for delivery of water-insoluble cancer drugs, J. Am. Chem. Soc. 130 (2008) 10876–10877.
[3] H.-P. Jia, D.R. Dreyer, C.W. Bielawski, Graphite oxide as an auto-tandem oxidation–hydration–aldol coupling catalyst, Adv. Synth. Catal. 353 (2011) 528–532.
[4] D.R. Dreyer, C.W. Bielawski, Carbocatalysis: heterogeneous carbons finding utility in synthetic chemistry, Chem. Sci. 2 (2011) 1233–1240.
[5] Q. Mei, Z. Zhang, Photoluminescent graphene oxide ink to print sensors onto microporous membranes for versatile visualization bioassays, Angew. Chem. Int. Ed. 51 (2012) 5602–5606.
[6] L. Tang, Y. Wang, Y. Li, H. Feng, J. Lu, J. Li, Preparation, structure, and electrochemical properties of reduced graphene sheet films, Adv. Funct. Mater. 19 (2009) 2782–2789.
[7] R.S. Sundaram, C. Gómez-Navarro, K. Balasubramanian, M. Burghard, K. Kern, Electrochemical modification of graphene, Adv. Mater. 20 (2008) 3050–3053.
[8] C.N.R. Rao, A.K. Sood, R. Voggu, K.S. Subrahmanyam, Some novel attributes of graphene, J. Phys. Chem. Lett. 1 (2010) 572–580.
[9] T.S. Sreeprasad, S.M. Maliyekkal, K.P. Lisha, T. Pradeep, Reduced graphene oxide–metal/metal oxide composites: facile synthesis and application in water purification, J. Hazard. Mater. 186 (2011) 921–931.
[10] T. Liu, Y. Li, Q. Du, J. Sun, Y. Jiao, G. Yang, Z. Wang, Y. Xia, W. Zhang, K. Wang, H. Zhu, D. Wu, Adsorption of methylene blue from aqueous solution by graphene, Colloids Surf. B 90 (2012) 197–303.
[11] W. Hu, C. Peng, M. Lv, X. Li, Y. Zhang, N. Chen, C. Fan, Q. Huang, Protein corona-mediated mitigation of cytotoxicity of graphene oxide, ACS Nano 5 (2011) 3693–3700.
[12] M.D. Stoller, S. Park, Y. Zhu, J. An, R.S. Ruoff, Graphene-based ultracapacitors, Nano Lett. 8 (2008) 3498–3502.
[13] F. Li, Y. Bao, J. Chai, Q. Zhang, D. Han, L. Niu, Synthesis and application of widely soluble graphene sheets, Langmuir 26 (2010) 12314–12320.
[14] Y. Zhu, S. Murali, W. Cai, X. Li, J.W. Suk, J.R. Potts, R.S. Ruoff, Graphene and graphene oxide: synthesis, properties, and applications, Adv. Mater. 22 (2010) 3906–3924.
[15] O.C. Compton, B. Jain, D.A. Dikin, A. Abouimrane, K. Amine, S.T. Nguyen, Chemically active reduced graphene oxide with tunable C/O ratios, ACS Nano 5 (2011) 4380–4391.
[16] T.S. Sreeprasad, T. Pradeep, Graphene for environmental and biological application, Int. J. Mod. Phys. B 26 (2012) 1242001–1242026.
[17] V. Chandra, J. Park, Y. Chun, J.W. Lee, I.-C. Hwang, K.S. Kim, Water-dispersible magnetite-reduced graphene oxide composites for arsenic removal, ACS Nano 4 (2010) 3979–3986.
[18] H. Gao, Y. Sun, J. Zhou, R. Xu, H. Duan, Mussel-inspired synthesis of polydopamine-functionalized graphene hydrogel as reusable adsorbents for water purification, ACS Appl. Mater. Interfaces 5 (2012) 425–432.
[19] H. Li, L. Zou, L. Pan, Z. Sun, Novel graphene-like electrodes for capacitive deionization, Environ. Sci. Technol. 44 (2010) 8692–8697.
[20] E.N. Wang, R. Karnik, Water desalination: graphene cleans up water, Nat. Nanotechnol. 7 (2012) 552–554.
[21] Z.-H. Huang, X. Zheng, W. Lv, M. Wang, Q.-H. Yang, F. Kang, Adsorption of lead(II) ions from aqueous solution on low-temperature exfoliated graphene nanosheets, Langmuir 27 (2011) 7558–7562.
[22] S.S. Gupta, T.S. Sreeprasad, S.M. Maliyekkal, S.K. Das, T. Pradeep, Graphene from sugar and its application in water purification, ACS Appl. Mater. Interfaces 4 (2012) 4156–4163.
[23] S. Simonich, R. Hites, Global distribution of persistent organochlorine compounds, Science 269 (1995) 1851–1852.
[24] B. Strandberg, R.A. Hites, Concentration of organochlorine pesticides in wine corks, Chemosphere 44 (2001) 729–735.
[25] B. Nagappa, G.T. Chandrappa, Mesoporous nanocrystalline magnesium oxide for environmental remediation, Microporous Mesoporous Mater. 106 (2007) 212–218.
[26] A.K. Leight, R.F. Van Dolah, Acute toxicity of the insecticides endosulfan, chlorpyrifos, and malathion to the epibenthic estuarine amphipod *Gammarus palustris* (Bousfield), Environ. Toxicol. Chem. 18 (1999) 958–964.
[27] B. Xuereb, P. Noury, V. Felten, J. Garric, O. Geffard, Cholinesterase activity in gammarus pulex (*Crustacea amphipoda*): characterization and effects of chlorpyrifos, Toxicology 236 (2007) 178–189.
[28] M.E. DeLorenzo, L.A. Taylor, S.A. Lund, P.L. Pennington, E.D. Strozier, M.H. Fulton, Toxicity and bioconcentration potential of the agricultural pesticide endosulfan in phytoplankton and zooplankton, Arch. Environ. Contam. Toxicol. 42 (2002) 173–181.
[29] J. Franzaring, L.J.M. van der Eerden, Accumulation of airborne persistent organic pollutants (POPs) in plants, Basic Appl. Ecol. 1 (2000) 25–30.
[30] S.L. Simonich, R.A. Hites, Organic pollutant accumulation in vegetation, Environ. Sci. Technol. 29 (1995) 2905–2914.
[31] E. Aoustin, A.I. Schäfer, A.G. Fane, T.D. Waite, Ultrafiltration of natural organic matter, Sep. Purif. Technol. 22–23 (2001) 63–78.
[32] J. Xu, L. Wang, Y. Zhu, Decontamination of bisphenol A from aqueous solution by graphene adsorption, Langmuir 28 (2012) 8418–8425.
[33] S.M. Maliyekkal, T.S. Sreeprasad, D. Krishnan, S. Kouser, A.K. Mishra, U.V. Waghmare, T. Pradeep, Graphene: a reusable substrate for unprecedented adsorption of pesticides, Small 9 (2013) 273–283.
[34] X. Liu, H. Zhang, Y. Ma, X. Wu, L. Meng, Y. Guo, G. Yu, Y. Liu, Graphene-coated silica as a highly efficient sorbent for residual organophosphorus pesticides in water, J. Mater. Chem. A 1 (2013) 1875–1884.
[35] Q. Wu, G. Zhao, C. Feng, C. Wang, Z. Wang, Preparation of a graphene-based magnetic nanocomposite for the extraction of carbamate pesticides from environmental water samples, J. Chromatogr. A 1218 (2011) 7936–7942.
[36] S. Sen Gupta, I. Chakraborty, S.M. Maliyekkal, T. Adit Maark, D.K. Pandey, S.K. Das, T. Pradeep, Simultaneous dehalogenation and removal of persistent halocarbon pesticides from water using graphene nanocomposites: a case study of lindane, ACS Sustainable Chem. Eng. 3 (2015) 1155–1163.
[37] W.S. Hummers, R.E. Offeman, Preparation of graphitic oxide, J. Am. Chem. Soc. 80 (1958) 1339.
[38] Y. Si, E.T. Samulski, Synthesis of water soluble graphene, Nano Lett. 8 (2008) 1679–1682.
[39] D. Li, M.B. Muller, S. Gilje, R.B. Kaner, G.G. Wallace, Processable aqueous dispersions of graphene nanosheets, Nat. Nano 3 (2008) 101–105.
[40] K. Haubner, J. Murawski, P. Olk, L.M. Eng, C. Ziegler, B. Adolphi, E. Jaehne, The route to functional graphene oxide, ChemPhysChem 11 (2010) 2131–2139.
[41] K.A.S. Fernando, V.G. Watson, X. Wang, N.D. McNamara, M.C. JoChum, D.W. Bair, B.A. Miller, C.E. Bunker, Migration of silver nanoparticles from silver decorated graphene oxide to other carbon nanostructures, Langmuir 30 (2014) 11776–11784.
[42] B. Andryushechkin, K. Eltsov, V. Shevlyuga, V.Y. Yurov, Direct STM observation of surface modification and growth of AgCl islands on Ag (1 1 1) upon chlorination at room temperature, Surf. Sci. 431 (1999) 96–108.
[43] V.K. Kaushik, XPS core level spectra and Auger parameters for some silver compounds, J. Electron. Spectrosc. Relat. Phenom. 56 (1991) 273–277.
[44] S.Y. Lagergren, Zur Theorie der sogenannten Adsorption gelöster Stoffe (1898).
[45] Y.S. Ho, G. McKay, The kinetics of sorption of divalent metal ions onto sphagnum moss peat, Water Res. 34 (2000) 735–742.
[46] Y.-S. Ho, Review of second-order models for adsorption systems, J. Hazard. Mater. 136 (2006) 681–689.